RSC Advances

ROYAL SOCIETY OF CHEMISTRY

www.rsc.org/advances

Journal Name

ARTICLE

Polyethersulfone (PES)/Cellulose Acetate Butyrate (CAB) Composite Hollow Fiber Membranes for BTEX Separation from Produced Water

Shangwen Zha [a, b], Jianjia Yu [a, *], Guoyin Zhang [a], Ning Liu [a] and Robert Lee [a]

Received 00th January 20xx,
Accepted 00th January 20xx

DOI: 10.1039/x0xx00000x

www.rsc.org/

Polyethersulfone (PES)/cellulose acetate butyrate (CAB) composite hollow fiber membranes were prepared by dry-jet wet-spinning for BTEX (benzene, toluene, ethylbenzene and xylene) separation from oilfield produced water. The effects of pore agent contents and air gaps on hollow fiber membrane morphology, permeate water flux, BTEX rejection efficiency and especially, membrane antifouling ability were investigated. It was found that the inner layer surface of the PES/CAB hollow fiber membrane became thicker and more porous with the increase of air gap size. When the air gap reached 4 cm, a very dense skin layer formed at the outer surface of the membrane. As the pore formation agent content increased from 1% to 5%, the specific surface area, pore size and permeate water flux of the membrane all increased, although rejection efficiency was slightly sacrificed. Our results also revealed that membranes prepared with larger air gaps showed a higher fouling tendency, and those with lesser air gaps exhibited better antifouling ability. The PES/CAB hollow fiber membrane prepared with 5% pore formation agent and 4 cm air gap showed 82.1–84.6% rejection of BETX accompanied by favourable permeate water flux, which is promising for the potential application in BTEX removal from produced water.

Introduction

Crude oil and natural gas production worldwide generates large quantity of produced water [1]. Produced water contains various kinds of contaminants, such as dissolved solids and dissolved /dispersed oil and grease. The discharge of produced water can cause serious damage to soil and water[2]. Various methods have been applied to remove the solid components in produced water such as electrocoagulation, sedimentation, and floatation[3-5]. However, the removal of dissolved oil and grease from produced water confronts producers with more challenges, especially for the removal of trace dissolved hydrocarbons, such as benzene, toluene, ethylbenzene and xylene (BTEX).

Maria Aivalioti *et al.* [6] introduced a raw, thermally treated lignite for BTEX adsorption, which exhibits a high contaminants adsorption capacity, but cannot be regenerated for further recyclable use. Prenafeta-Boldu *et al.* [7] investigated biodegradation of BTEX with fungus, but the introduction of fungal strains into water may cause other problems such as biological pollution. Michael *et al.* [8] reported a field test of surfactant-modified zeolite for BTEX removal, but the BTEX separation efficiency was proved to be effective only at the beginning of the test, and the breakdown of zeolite occurred after two rounds of operation/regeneration, which results in a low permeability and high pressure requirement.

In the past few years, membrane separation technology has been widely applied for water treatment[9-11]. Different kinds of membranes have been used for the separation of particles and molecules such as bacterial[12], drug[13], crude oil[14], palm oil [15] and commercial machine oil [16]. Liu *et al.* [17] reported a MFI-type zeolite membrane for produced water treatment through reverse osmosis. It was shown that a high BTEX separation efficiency (>95%) was achieved together with a sacrificed water flux (0.3-0.5 $kg \bullet m^{-2} \bullet h^{-1}$). The large-scale application of membrane separation is usually challenged with the trade-off between water flux and rejection efficiency. In addition, membrane fouling always takes place during a long-term membrane operation. Especially in the case of BTEX removal, because the molecular sizes of dissolved BTEX in produced water are much smaller than those of the multicomponent oil dispersed in water, a membrane with smaller pore size is supposed to be required

[a] *Petroleum Recovery Research Center, New Mexico Institute of Mining and Technology, Socorro, NM 8780, United States.*
[b] *Materials Engineering Department, New Mexico Institute of Mining and Technology, Socorro, NM, 87801, United States.*
[*] *Corresponding author. Tel: +01-575-8355570; Email: yu@nmt.edu (J. Yu).*

Electronic Supplementary Information (ESI) available: Fig. S1 to Fig. S4 shows cross sectional images of all the composite PES/CAB hollow fiber membranes examined at different resolution. See DOI: 10.1039/x0xx00000x

for effective BTEX removal; this, however, will lead to sacrificed water flux and thus a low water treatment capacity. On the other hand, the tendency of membrane fouling becomes more significant when dealing with these traceable organic contaminants.

Recently, membrane wettability modification and pore size designation have been considered as an efficient way to simultaneously improve membrane separation performance and antifouling ability. Cellulose-based ester is a type of highly hydrophilic polymer that has been commonly reported in membrane hydrophilicity modification. Rahimpour *et al.* [18] prepared flat-sheet polyethersulphone (PES)/ cellulose acetate phthalate (CAP) membranes by phase inversion. Their PES/CAP flat-sheet membrane showed good protein and heavy metal ions rejection as well as improved antifouling ability compared to the membrane that was prepared with PES only. Cellulose acetate butyrate (CAB) is another kind of cellulose ester; compared to CAP, the CAB contains longer and smaller liner ester group, which is believed to have good internal plasticization and thus better miscibility with PES. Even small amounts of CAB could effectively improve the hydrophilicity of the PES membrane [19].

Pore size distribution in hollow fiber membranes is not only dependent on the raw polymeric materials used for hollow fiber membrane fabrication, but also the parameters for the dry-jet wet-spin technique, i.e., dope concentration, bore fluid composition, fiber collection rate, type and concentration of pore agents and air gap distances. The study of pore formation agents and air gaps has recently gained much attention. Myeong-Jin Han [20] investigated the effect of polyvinylpyrrolidone (PVP) contents on the morphology of flat polysulfone (PSF) membranes prepared with phase inversion method. It was found that the right amount of PVP can accelerate the phase inversion speed in the porous layer of the membrane, and lead to larger pore size by inducing polymer molecules to collapse. However, an excessive amount of PVP led to a sharp increase of dope solution viscosity and inhibited its phase inversion efficiency. Tai Shun Chung et al. [21] investigated the effect of air gaps on membrane properties. They found that the outer membrane layer could bear more stress load than the inner layer within the air gap distance. With an increase of air gap, the stress loaded on the outer layer helps form a top skin layer on the outer surface of the membrane due to molecule orientation and packaging. M. Khayet [22] prepared polyvinylidene fluoride (PVDF) hollow fiber membranes with the air gap varying from 1 to 80 cm. Their results showed that a membrane prepared with a larger air gap tended to form a dense outer layer with small pores, and the membrane thickness was not obviously affected by the air gap. M. Khayet's research also revealed that the rejection efficiency of membrane was controlled by the inner surface of the membrane with a small air gap but the outer surface controlled rejection efficiency in a membrane with a large air gap. Today, the inconsistency still exists for the air gap influences on membrane morphology and property[21, 23-25].

In this study, we prepared a series of PES/CAB composite hollow fiber membranes with different PVP contents and air gaps by using the dry-jet wet-spin method. The effects of PVP contents and air gaps on hollow fiber membrane pore size and pore size distribution, membrane fouling tendency, water flux, BTEX removal efficiency and especially the antifouling ability was systematically investigated. It was expected that this study would reveal the relationship among membrane fabrication parameters, BTEX separation efficiency and membrane anti-fouling ability.

Experimental

Materials

Polyethersulfone (PES, Veradel® A-301) in pellet was provided by Solvay Company. Regent grade N-methyl-2-pyrrolidone (NMP, >98%), cellulose acetate butyrate (CAB, M_n~30,000) and Polyvinylpyrrolidone (PVP 40, M_n~40,000) were purchased from Sigma-Aldrich for hollow fiber membrane preparation. Hexane (anhydrous, 95%) and methanol (anhydrous, 99.8%) were also purchased from Sigma-Aldrich for post hollow fiber membrane treatment without further purification.

Polymer dope preparation and hollow fiber membrane fabrication

To prepare polymer dope solution, pre-dried PES was first dissolved in NMP solution under continuous stirring for eight hours until it became homogeneous. Then, CAB and PVP were added into the PES/NMP suspension for another 12 hours mixing. The obtained light-yellow homogeneous dope solution was degassed overnight in a vacuum oven for further use. Hollow fiber membranes were prepared with the dry-jet wet spin method; the details of membrane fabrication have been described elsewhere [22]. The prepared hollow fiber membranes were first immersed in DI water followed by methanol and hexane to gradually remove residual water and residual solvent (NMP) inside the membrane. This procedure also reduces the effect of surface tension during the drying process, and minimizes fiber deformation and pore collapse before drying at room temperature [26]. Table 1 shows hollow fiber membranes fabricated with different dope compositions. M0 refers to the hollow fiber membrane fabricated with neat PES.

Membrane morphology and pore size distribution

To observe the morphology of the PES/CAB hollow fiber membrane, the dried hollow fiber membranes were broken in liquid nitrogen and then sputtered with platinum. The cross section, inner surface and outer surface of hollow fiber membranes were examined by scanning electron microscopy

(SEM, S3200N, Hitachi). The accelerating voltage for SEM characterization was 25.0 kV.

Table 1. Spinning Parameters of the Hollow Fiber Membranes

Membrane	M0	M1	M2	M3	M4	M5	M6	M7	M8	M9
PES/CAB content (ω %)	29/0			27.26/1.74						
PVP content (ω %)	5	1	1	1	3	3	3	5	5	5
Bore fluid composition(g/g)	NMP/water(90/10)									
External coagulation bath	Water(25°C)									
Air gap(cm)	2	2	3	4	2	3	4	2	3	4
Dope solution flow rate(ml/min)	2									
Bore solution flow rate(ml/min)	1									
Collecting velocity(cm/min)	422									

Pore size and pore size distribution measurements were obtained with a BET surface area analyzer (ASAP2020, Micromeritics, USA). Pore size distribution was calculated according to the nitrogen desorption isotherm. The relationship between the Kelvin radiuses (critical radius) and relative pressure was represented by the classical Kelvin equation expressed as follows [27]:

$$\text{Log}\,(P/P_0) = \frac{-4.14}{r_k} \quad (1)$$

where r_k is kelvin radius (critical radius) in Å and P/P_0 is the relative pressure during the surface area measurement.

Permeate water flux and BTEX rejection

Hollow fiber membrane modules were prepared with epoxy potting technique. Briefly, 10 hollow fibers were placed into a stainless steel tube with both ends sealed with epoxy, leaving an effective length of 22 cm. Permeate water flux was first measured by injecting DI water through the membrane module under different back pressures ranging from 40 psi to 100 psi. Afterwards, 500 ppm benzene, 300 ppm toluene, 150 ppm ethyl benzene and 150 ppm xylene were prepared as feed solutions to estimate BTEX removal efficiency of the membranes. The BTEX concentrations of feed solutions and permeated water were measured by total carbon analysis (Shimadzu, TOC-L CSH, Japan). Permeate water flux (PWF) and BTEX rejection efficiency of hollow fiber membranes were obtained with Eqs. (2) and (3), respectively.

$$J_w = \frac{Q}{A \times T} \quad (2)$$

$$R = \frac{C_f - C_p}{C_f} \times 100\% \quad (3)$$

where, J_w is the PWF of the membrane (L/m^{2}h), Q represents the volume of permeated water (L), A is the effective area of the membrane (m^2) and T is the permeation time (hour). R is rejection efficiency (%). C_f and C_p are the concentration (ppm) of the feed solutions and permeate water, respectively.

Antifouling ability measurement

Antifouling ability of the membrane was evaluated in terms of flux decline ratio (FDR) and flux recovery ratio (FRR) by using 1000 ppm benzene as feed solution. The benzene solution was first injected into the lumen side of the hollow fiber membranes for five hours, after which a forward DI water flushing was performed for hollow fiber membrane regeneration. In this study, FDR is defined as permeate water flux reduction of the hollow fiber membrane caused by benzene fouling, and the FRR indicates the regeneration capacity of hollow fiber membrane. FDR and FRR can be obtained by Eqs. (4) and (5),

$$FDR = \left(1 - \frac{J_p}{J_f}\right) \times 100\% \quad (4)$$

$$FRR = \frac{J_r}{J_f} \times 100\% \quad (5)$$

where J_f is the PWF of the fresh hollow fiber membrane, J_p and J_r are the PWFs of the contaminated membrane that were obtained before and after DI water regeneration, respectively.

Results and discussion

Membrane morphology

Fig. 1 shows SEM images of the cross section of hollow fiber membranes. It can be seen that the hollow fiber shows a typical structure with both finger-link pores and sponge-like pores. The details of membrane morphologies are listed in Electronic Supplementary Information (ESI). It can be seen in Fig. S1 and Fig. S2 that the diameter and thickness of the hollow fiber membranes were not affected by the PVP contents and air gaps. The outer side diameter and thickness of the membrane are around 575μm and 125 μm, respectively.

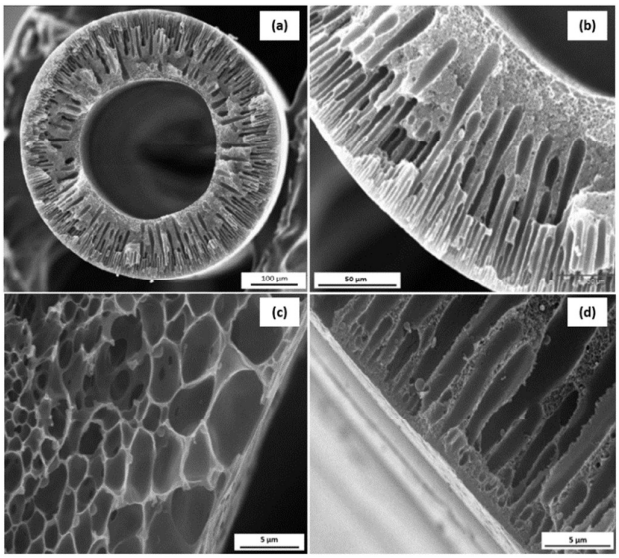

Fig. 1. Cross-sectional SEM images of PES/CAB hollow fiber membranes prepared at PVP content=3% and air gap=4 cm. (a and b) cross sectional overview; (c) cross section close to inner surface; (d) cross section close to outer surface.

Fig. S2 shows the cross section of all hollow fiber membranes examined at higher resolution (600×). Comparing Fig. S2(c) with Fig. S2 (a) and Fig. S2 (b), it can be seen that with a larger air gap, a thicker spongy-like inner layer without finger-like pores was formed in M3. A similar phenomenon was observed as well when comparing Fig. S2 (f) with Fig. S2 (d) and Fig. S2 (e), and comparing Fig. S2 (i) with Fig. S2 (g) and Fig. S2 (h). The generation of the thicker sponge-like inner layer of M3, M6 and M9 is probably due to the longer phase inversion process between dope solutions and bore fluid in the air. This result is well consistent with previous studies, which indicated that rapid demixing between non-solvent and dope solution makes the finger-like pores, while slow phase inversion promotes the sponge-like pores [28, 29].

Fig. S3 shows the pore structure of the inner layer of the membranes. There is no doubt that the pore size is dramatically increased with the increased addition of PVP. As an effective pore forming additive, PVP is widely used in preparing membranes and fibers to adjust pore size and pore size distribution, thus increasing membrane permeability [30]. In Fig. S3, it is also obvious that the pores in immediate proximity to the inner surface exhibit the largest pores for all the membranes. Comparing Fig. S3 (a), Fig. S3 (d) and Fig. S3 (g), all these membranes were fabricated with the air gap of 2cm. The pore size increased with the increase of PVP content, especially for the pores that located close to the surface of the very inner surface. This phenomenon could be explained by the competition between polymer dissolution and phase inversion that both taken place on the inner surface. Since the bore fluid comprises 90 wt% NMP, the phase inversion process is much slower than the dissolution of PES or PES/CAB in NMP. The big pores on the very inner surface may be the result of strong NMP dissolving and weak water setting. Fig. S4 depicted the morphology of selective layer on the outer surfaces of the membranes. It can be seen that, when air gap is 2cm, the pores near the outer surface were mostly open ended. When air gap increased to 4 cm, dense skin layers were formed on the outer surfaces of membrane M3, M6 and M9. This phenomenon was probably caused by the greater molecule orientation and thus tighter molecular chain packing due to the larger air gap, as reported by Chung T S et al [21].

Fig. 2 shows the pore size distributions of PES and PES/CAB hollow fiber membranes. It is obvious in Fig. 2 (a) that the pore diameter is around 4.3 nm for most of the spores in membrane M4. As the air gaps increased to 3 cm and 4 cm, smaller pores were generated in membrane M5 and M6. The pore diameters are 2.9 nm and 0.8 nm, respectively. While in Fig. 2 (b), compared to membrane M1, the peaks of the pore size distribution curves for M4 and M7 both shifted to the right. This shift can be contributed by the increase of PVP content. The PVP is able to induce polymer molecules collapse and facilitate the formation of large pores within the membranes [20].

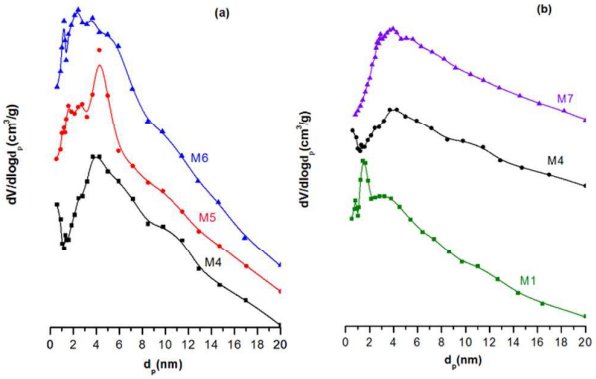

Fig. 2. Differential pore size distribution of the membranes (a: M4, M5, M6; b: M1, M4, M7).

Water flux and BTEX rejection

BET-specific surface area and pure water flux of the membranes tested at 100 psi were listed in Table 2. It can be seen that the specific surface areas of the membranes decreased with the increase of air gaps and increased with the increase of PVP contents. The increase of air gap led to smaller pore size but not higher specific area. It is probably because of the decreased total pore volume caused by molecule orientation and the increase of pore size on the inner surface caused by longer time of phase inversion. In Table 2, there is a significant permeate water flux improvement of the membrane with a slight increase of specific surface area. As the PVP content increased from 1% to 5%, the permeate water flux of the membranes prepared

with the same air gaps improved significantly from 1.45L/m^{2}h to 19.48L/m^{2}h. For membranes prepared with the same PVP content, the PWF of the membranes decreased with the increase of air gap. Rejection efficiencies of hollow fiber membranes toward BTEX at 100 psi are listed in Table 3. On one hand, it can be seen that the rejection efficiency of BETX decreased with the increase of PVP content, while it increased with the increase of air gap.

Table 2. Pure water flux of the composite hollow fiber membranes

Membrane	Specific surface area(m^2/g)	Pure water flux(L/m^{2}h)
M1	12.71	1.45
M2	11.95	1.26
M3	8.51	1.17
M4	14.35	10.75
M5	14.06	8.16
M6	12.49	1.35
M7	19.13	19.48
M8	16.26	17.32
M9	14.98	16.26

Table 3. Separation efficiency of the hollow fiber membranes

Membrane	Rejection efficiency (%)			
	Benzene	Toluene	Ethylbenzene	Xylene
M0	71.8	73.9	74.3	73.5
M1	91.1	92.7	93.6	94.7
M2	93.2	97.6	98.4	96.7
M3	97.5	98.6	99.2	98.1
M4	71.6	76.6	78.6	78.8
M5	78.2	81.3	86.2	87.4
M6	85.5	91.5	93.7	92.3
M7	70.3	71.1	70.4	71.5
M8	74.2	76.5	78.7	79.2
M9	82.1	84.6	83.2	84.1

The variation of rejection efficiency is consistent with the changes of membrane morphology, pore size distribution and specific surface area. The higher PVP content not only increased pore size of the hollow fiber membrane, but also facilitated the movement of organic molecules from the lumen side to the outer surface of the membrane. On the other hand, compared to the neat PES hollow fiber membrane (M0), the PES/CAB composite hollow fiber membrane exhibits higher BTEX rejection efficiency except M7. The M0 possessed the highest hydrophobicity in all 10 batches of membranes, which means more organic molecules tend to be adsorbed on the membrane surface, and result in higher apparent rejection efficiency comparing with M7.

Fig. 3 shows the permeate water flux of M0, M7, M8 and M9. It was obvious that the permeate water flux of the membranes increased with the increase of pressure. The neat PES hollow fiber membrane M0 showed the lowest permeate water flux at all pressures due to its lowest hydrophilicity. It also shows the rejection efficiency of the hollow fiber membranes toward 500ppm benzene solution at different pressures in Fig. 3. On one hand, it can be seen that the rejection efficiency of the membranes decreased with the increase of pressure. The rejection efficiency of the membrane was determined by the competition of penetration of organic molecules and that of water. In this study, it seems that higher pressure facilitated more penetration of organic molecules than that of water, and thus led to the apparent decline of rejection with the increase of pressure. On the other hand, the rejection of M7, M8 and M9 increased with the increase of air gap at all testing pressures. It is interesting to note that M0 showed higher rejection than M7 but lower rejection than M8 and M9. This can be explained by the synergic effects of high hydrophobicity and large pore size of the membrane M0, as revealed in our previous work [31].

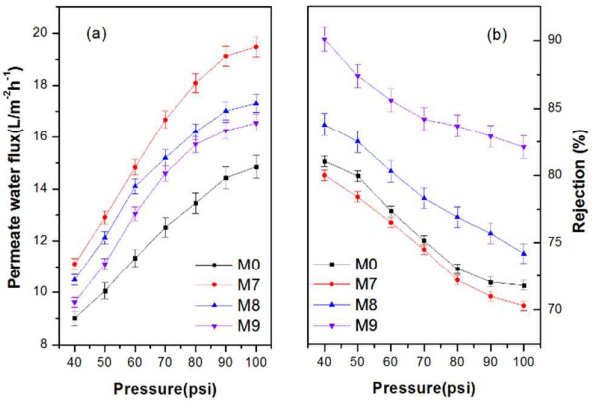

Fig. 3. (a) Permeate water flux and (b) rejection efficiency of 500 ppm benzene as a function of pressure.

Antifouling performance

For membrane technology based water purification process, the decline of permeate water flux is mostly caused by membrane fouling. To evaluate the antifouling ability of our hollow fiber membranes, the relationship between permeate water flux and operation time was examined in details. The results were plotted in Fig. 4. It was clear that M0 showed the lowest permeate water flux at all operation times, and the permeate water flux declined with operation time. For membranes M7, M8 and M9, all membranes exhibited improved permeate water flux, but the flux decreased with the increase of permeation time as well. Once the separation process started, benzene molecules tended to attach to the inner surface of the hollow fiber membrane. In the first 30 minutes, since the adsorbed benzene molecules occupied only a small portion of the total pore volumes in the hollow

fiber membrane, there was almost no effect on the permeate water flux. With the operation time increased to 60 minutes, more benzene molecules were supposed to attach to the membrane inner surface, and thus resulted in an obvious permeate water flux decline, as seen in Fig. 4(a), where the most significant permeate water flux drop occurred when the operation time was 60 minutes. With the experiment continuously running, the membrane inner surface was gradually saturated with benzene molecules.

Fig. 4. (a) Permeate water flux and (b) differential permeate water flux as a function of operation time

During the saturation process, partial benzene molecules from newly injected feed solution persistently attached to

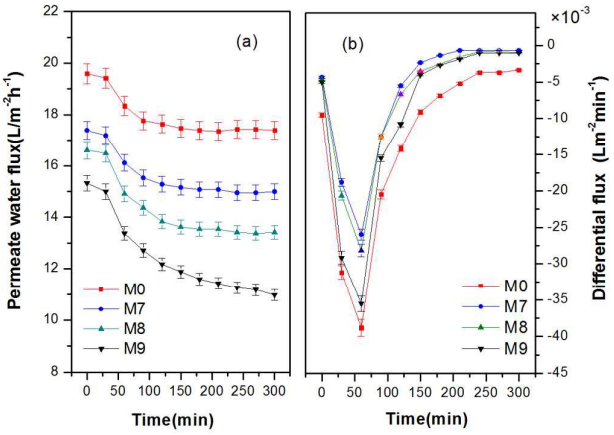

the membrane's inner surface, while partial already-attached benzene molecules were flushed away from the membrane inner surface by hydraulic flow of the feed solution. For membranes M7, M8 and M9, in the first 240 minutes of operation, the amount of adsorbed benzene molecules was greater than the amount desorbed, that was caused by hydraulic flow, which led to a further decrease of permeate water flux. After 240 minutes of the test, the adsorption and desorption of benzene molecules seemed to be at the same level, and the total benzene molecules on the membrane inner surface remained dynamically stable. As a result, the permeate water flux stopped declining for the rest of the test. While membrane M0 showed continuous permeate water flux decline after 240 minutes of the test, it can be explained through its relatively higher hydrophobicity compared to the membranes M7, M8 and M9.

The differential permeate water fluxes (DPWF) of all the hollow fiber membranes are also plotted in Fig. 4(b). It can be seen that all the membranes exhibited negative differential permeate water flux, which indicated an actual decrease of permeate water flux. M0 showed the lowest differential permeate water flux at all the operation times, and all the differential permeate water fluxes remained negative even after 300 minutes of operation. In addition, it is obvious in Fig. 4 that the antifouling ability of the PES/CAB hollow fiber membrane can be ranked as M7>M8>M9. Here it is necessary to note that the membranes M7, M8 and M9 were fabricated under the air gaps of 2 cm, 3 cm and 4 cm, respectively, and the pore size at the inner surface of the hollow fiber membranes increased with the air gap, as previously shown in Fig. S3 (g), (h) and (i). It is well accepted that increased pore size can lead to an improved roughness of the membrane surface [32], and the improved roughness can lead to higher fouling tendency [33]. This is why the M7 showed the best antifouling ability among the series of PES/CAB hollow fiber membranes.

Table 4. Flux Decay Ratio and Flux Recovery Ratio of the hollow fiber membranes.

Membrane	FDR (%)	FRR (%)
M0	27.9	73.6
M7	12.1	95.7
M8	13.5	93.6
M9	18.7	82.9

Table 4 listed the permeate water flux decay ratio as well as flux recovery ratio of M0, M7, M8 and M9. It can be seen that M0 showed the highest flux decay ratio and the lowest flux recovery ratio, indicating its highest fouling tendency and lowest recovery ability by water flushing. Furthermore, hollow fiber membranes prepared with smaller air gap tended to show lower flux decline ratio and higher flux recovery ratio, and the membrane exhibited a higher antifouling ability. In addition, it was found that with 1.74% of CAB in PES dope solution, the membrane M7 showed a decrease of FDR by 15.8% and an increase of FRR by 22.1%, compared with membrane M0 prepared without CAB, which indicated the high efficiency of CAB in improving the antifouling ability of hollow fiber membranes.

Conclusions

In summary, a series of PES/CAB composite hollow fiber membranes were prepared with different PVP contents and air gaps for the removal of dissolved BETX from produced water. The morphology and performance of the membranes were systematically characterized and compared with each other. There is a very thin top skin layer formed on the outer surface of the hollow fiber membrane, as well as a thick but more porous inner surface layer that appeared when the air gap was 4 cm. BET results revealed that pore size distribution of the composite membranes shifted to larger pore size zones with an increase in PVP content from 1% to 3%. The results of membrane separation performance illustrated that the outer skin layer was effective for improving the BTEX rejection efficiency, but that it could also cause a decrease in permeate water flux. The membrane prepared with greater air gaps showed higher fouling tendency, and the membrane with lesser air gaps exhibited better antifouling ability. The

antifouling ability test proved that the membranes prepared with CAB possess better antifouling ability and exhibit lower permeate water flux decline rate and flux decay ratio, as well as higher flux recovery ratio.

Acknowledgements

This research is supported by the Research Partnership to Secure Energy for America (RPSEA) under its Small Producer Program, award number 12123-16. The authors appreciate the aid of Liz Bustamante for her assistance in editing this manuscript.

References

1. S. Alzahrani, A. W. Mohammad, N. Hilal, P. Abdullah and O. Jaafar, *Separation and Purification Technology*, 2013, **118**, 324-341.
2. A. Fakhru'l-Razi, A. Pendashteh, L. C. Abdullah, D. R. A. Biak, S. S. Madaeni and Z. Z. Abidin, *Journal of Hazardous Materials*, 2009, **170**, 530-551.
3. A. Akyol, O. T. Can, E. Demirbas and M. Kobya, *Separation and Purification Technology*, 2013, **112**, 11-19.
4. E. Ingall and R. Jahnke, *Geochimica et Cosmochimica Acta*, 1994, **58**, 2571-2575.
5. S. Liu, Q. Wang, H. Ma, P. Huang, J. Li and T. Kikuchi, *Separation and Purification Technology*, 2010, **71**, 337-346.
6. M. Aivalioti, D. Pothoulaki, P. Papoulias and E. Gidarakos, *Journal of Hazardous Materials*, 2012, **207–208**, 136-146.
7. F. X. Prenafeta-Boldú, H. Ballerstedt, J. Gerritse and J. T. C. Grotenhuis, *Biodegradation*, 2004, **15**, 59-65.
8. R. S. B. J. Michael Ranck, Jeffrey L. Weeber, Lynn E. Katz and Enid J. Sullivan, *Journal of Environmental Engineering*, 2005, **131**, 434-442.
9. C. Kappel, A. J. B. Kemperman, H. Temmink, A. Zwijnenburg, H. H. M. Rijnaarts and K. Nijmeijer, *Journal of Membrane Science*, 2014, **453**, 359-368.
10. R. J. Barnes, R. R. Bandi, F. Chua, J. H. Low, T. Aung, N. Barraud, A. G. Fane, S. Kjelleberg and S. A. Rice, *Journal of Membrane Science*, 2014, **466**, 161-172.
11. W.-P. Zhu, S.-P. Sun, J. Gao, F.-J. Fu and T.-S. Chung, *Journal of Membrane Science*, 2014, **456**, 117-127.
12. H. Ma, B. S. Hsiao and B. Chu, *Journal of Membrane Science*, 2014, **452**, 446-452.
13. K. Y. Wang and T.-S. Chung, *AIChE Journal*, 2006, **52**, 1363-1377.
14. X. S. Yi, S. L. Yu, W. X. Shi, N. Sun, L. M. Jin, S. Wang, B. Zhang, C. Ma and L. P. Sun, *Desalination*, 2011, **281**, 179-184.
15. X. Zhu, W. Tu, K.-H. Wee and R. Bai, *Journal of Membrane Science*, 2014, **466**, 36-44.
16. H.-J. Li, Y.-M. Cao, J.-J. Qin, X.-M. Jie, T.-H. Wang, J.-H. Liu and Q. Yuan, *Journal of Membrane Science*, 2006, **279**, 328-335.
17. N. Liu, L. Li, B. McPherson and R. Lee, *Journal of Membrane Science*, 2008, **325**, 357-361.
18. A. Rahimpour and S. S. Madaeni, *Journal of Membrane Science*, 2007, **305**, 299-312.
19. P. Kunthadong, R. Molloy, P. Worajittiphon, T. Leejarkpai, N. Kaabbuathong and W. Punyodom, *J Polym Environ*, 2015, **23**, 107-113.
20. M.-J. Han and S.-T. Nam, *Journal of Membrane Science*, 2002, **202**, 55-61.
21. T.-S. Chung and X. Hu, *Journal of Applied Polymer Science*, 1997, **66**, 1067-1077.
22. J. D. Wind, C. Staudt-Bickel, D. R. Paul and W. J. Koros, *Industrial & Engineering Chemistry Research*, 2002, **41**, 6139-6148.
23. F. Tasselli, J. C. Jansen, F. Sidari and E. Drioli, *Journal of Membrane Science*, 2005, **255**, 13-22.
24. P. Aptel, N. Abidine, F. Ivaldi and J. P. Lafaille, *Journal of Membrane Science*, 1985, **22**, 199-215.
25. J.-H. Kim, Y.-I. Park, J. Jegal and K.-H. Lee, *Journal of Applied Polymer Science*, 1995, **57**, 1637-1644.
26. A. G. F. Norman N. Li, W.S. Winston Ho and Takeshi Matsuura, *Advanced Membrane Technology and Applications*, John Wiley & Sons, 2011.
27. E. P. Barrett, L. G. Joyner and P. P. Halenda, *Journal of the American Chemical Society*, 1951, **73**, 373-380.
28. E. Fontananova, J. C. Jansen, A. Cristiano, E. Curcio and E. Drioli, *Desalination*, 2006, **192**, 190-197.
29. M. Rahbari-sisakht, A. F. Ismail and T. Matsuura, *Separation and Purification Technology*, 2012, **88**, 99-106.
30. S. Simone, A. Figoli, A. Criscuoli, M. C. Carnevale, A. Rosselli and E. Drioli, *Journal of Membrane Science*, 2010, **364**, 219-232.
31 S. Zha, J. Yu, G. Zhang, N. Liu and R. Lee. Polyethersulfone (PES)/Cellulose Acetate Butyrate (CAB) Hybrid Hollow Fiber Membranes for Organic Matter Removal from Produced Water. Paper SPE 173787-MS present at the SPE International Symposium on Oilfield Chemistry held in The Woodlands, Texas, USA, 13–15 April 2015.
32. W. Richard Bowen and T. A. Doneva, *Journal of Colloid and Interface Science*, 2000, **229**, 544-549.
33. G. Z. Ramon and E. M. V. Hoek, *Journal of Membrane Science*, 2013, **425–426**, 141-148.